



1 **Influence of long-term changes in solar irradiance forcing on the**  
2 **Southern Annular Mode**

3 Nicky M. Wright<sup>1,2,\*</sup>, Claire E. Krause<sup>1,3,+</sup>, Steven J. Phipps<sup>4</sup>, Ghyslaine Boschat<sup>5</sup>, Nerilie J. Abram<sup>1,2</sup>

4 <sup>1</sup> Research School of Earth Sciences, Australian National University, Canberra ACT 2601, Australia

5 <sup>2</sup> ARC Centre of Excellence for Climate Extremes, Australian National University, Canberra ACT 2601, Australia

6 <sup>3</sup> ARC Centre of Excellence for Climate System Science, Australian National University, Canberra ACT 2601, Australia

7 <sup>4</sup> Ikigai Research, Sandy Bay, Tasmania 7006, Australia

8 <sup>5</sup> Bureau of Meteorology and ARC Centre of Excellence for Climate Extremes, Melbourne, Victoria 3001, Australia

9

10 *Correspondence to:* Nicky M. Wright ([nicky.wright@sydney.edu.au](mailto:nicky.wright@sydney.edu.au))

11 *\*Current address:* School of Geosciences, University of Sydney, NSW 2006, Australia

12 *+Current address:* Geoscience Australia, Canberra ACT, Australia

13

14

15 **Abstract.** The Southern Annular Mode (SAM) is the leading mode of climate variability in the extratropical  
16 Southern Hemisphere, with major regional climate impacts. Observations, reconstructions, and historical climate  
17 simulations all show positive trends in the SAM since the 1960s; however, earlier trends in palaeoclimate SAM  
18 reconstructions cannot be reconciled with last millennium simulations. Here we investigate the sensitivity of the  
19 SAM to solar irradiance variations using simulations with a range of constant solar forcing values, and last  
20 millennium transient simulations with varying amplitude solar forcing scenarios. We find the mean SAM state can  
21 be significantly altered by solar irradiance changes, and that transient last millennium simulations using a high-  
22 amplitude solar scenario have an improved and significant agreement with proxy-based SAM reconstructions.  
23 Our findings suggest that the effects of solar forcing on high-latitude climate may not be adequately incorporated  
24 in most last millennium simulations, due to solar irradiance changes that are too small and/or the absence of  
25 interactive atmospheric chemistry in global climate models.

26

27

28 **1 Introduction**

29 The evolution of climate over the last millennium provides a unique setting for determining how modes of climate  
30 variability respond to natural and anthropogenic forcing. The temporal evolution of external forcings (such as  
31 atmospheric greenhouse gas concentrations, volcanic eruptions and changes in solar irradiance) is reasonably  
32 well understood over the last millennium (Schmidt et al., 2011; Schmidt et al., 2012; Jungclaus et al., 2017),  
33 allowing their effects on climate to be explored using global climate models. Such simulations have primarily  
34 been compared to proxy-based reconstructions of global or hemispheric mean temperature (Neukom et al.,  
35 2018; Neukom et al., 2019), or analysed for changes in tropical or Northern Hemisphere modes of climate  
36 variability (Ortega et al., 2015; Otto-Bliesner et al., 2016). There is considerably less palaeoclimate data available  
37 in the Southern Hemisphere (Emile-Geay et al., 2017), and investigations into the influence of external forcings on  
38 Southern Hemisphere climate variability are scarce. Despite this, evidence exists that major changes in Southern



39 Hemisphere climate variability occurred during the last millennium, including via the Southern Annular Mode  
40 (SAM) (Abram et al., 2014; Dätwyler et al., 2018).

41 The SAM, also known as the Antarctic Oscillation (AAO), is the leading pattern of atmospheric variability  
42 in the extratropical Southern Hemisphere. SAM variability describes changes in the strength and position of the  
43 westerly wind belt (or mid-latitude westerly jet) over the Southern Ocean, and is represented by zonally opposing  
44 geopotential height anomalies between the mid (~40°S) and high (~65°S) latitudes (Thompson and Wallace, 2000;  
45 Marshall, 2003). A positive phase of the SAM is characterised by negative pressure anomalies over Antarctica  
46 compared to positive pressure anomalies at mid-latitudes (Marshall, 2003), and a poleward contraction of the  
47 westerly jet. Changes in the SAM have important impacts on temperature and precipitation across the Southern  
48 Hemisphere, with particularly strong influences on weather across Australia, New Zealand, South America,  
49 southern Africa and Antarctica (Gillett et al., 2006; Sen Gupta and England, 2006; Hendon et al., 2007). For  
50 example, a positive SAM is associated with cool and wet conditions across most of southern Australia (excluding  
51 Tasmania) (Gillett et al., 2006; Sen Gupta and England, 2006; Hendon et al., 2007; Fogt and Marshall, 2020), cool  
52 and dry conditions across the Antarctic continent contrasted with warm and wet conditions along the Antarctic  
53 Peninsula (Fogt and Marshall, 2020), and warm and dry conditions in New Zealand, Tasmania, and southern  
54 South America (Gillett et al., 2006).

55 Characterisation of the SAM over the past century has relied on observational records and/or reanalysis  
56 modelling (Marshall, 2003; Fan and Wang, 2004; Fogt et al., 2009; Visbeck, 2009). Short and sparse Antarctic  
57 climate observations mean that SAM variability is directly measured only since 1957 (Marshall, 2003). Seasonal  
58 SAM reconstructions from limited observations, primarily in the mid-latitudes, extend the instrumental record  
59 back to 1865 for austral summer/autumn, and 1905 for winter (Fogt et al., 2009; Jones et al., 2009). Observations  
60 and reanalyses have shown a robust positive trend in the SAM since the mid-20th Century that is most  
61 pronounced in summer (Marshall, 2003; Fogt and Marshall, 2020), and has been primarily linked to the depletion  
62 of stratospheric ozone (Thompson and Solomon, 2002; Gillett and Thompson, 2003; Son et al., 2009; Polvani et  
63 al., 2011a; Thompson et al., 2011; Grise et al., 2013; Jones et al., 2016; Banerjee et al., 2020), with contributions  
64 from increasing atmospheric greenhouse gases and internal variability/tropical decadal variability (e.g., Fyfe et al.,  
65 1999; Kushner et al., 2001; Shindell and Schmidt, 2004; Arblaster and Meehl, 2006; Yang et al., 2020). During all  
66 other seasons, the positive SAM trends have been mainly attributed to increasing greenhouse gases (year-round  
67 trends) (Polvani et al., 2011b; Thompson et al., 2011). Analysis of historical simulations from the fifth Coupled  
68 Model Intercomparison Project (CMIP5) has also found a significant response of the SAM in all seasons to solar  
69 forcing, however the amplitude of this response is small compared to internal variability and anthropogenic  
70 forcing, and unlikely to be identifiable in observations (Gillett and Fyfe, 2013). Future climate simulations suggest  
71 that increasing greenhouse gases will cause further positive trends in the SAM (e.g., Wang and Cai, 2013; Gillett  
72 and Fyfe, 2013; Goyal et al., 2021). In summer the trends are more uncertain as the changes in SAM will depend  
73 on the opposing forcing from ozone recovery (Banerjee et al., 2020) and increasing greenhouse gases (Arblaster  
74 et al., 2011; Meehl et al., 2012; Barnes and Polvani, 2013). The positive trend in austral summer SAM has paused  
75 since the 2000s due to stratospheric ozone recovery resulting from the Montreal Protocol (Banerjee et al., 2020).



76 Palaeoclimate proxies (i.e., ice cores, tree-rings, stalagmites, corals, lake records, etc.) have been used  
77 to reconstruct the SAM back through time, presenting a long-term picture of the natural variability of the SAM  
78 prior to recent anthropogenic forcing (Abram et al., 2014; Dätwyler et al., 2018; Saunders et al., 2018; Villalba et  
79 al., 2012). Proxy-based reconstructions indicate that the SAM experiences a large amount of natural variability  
80 that may be intrinsic (unforced) or a response to natural external forcing, while SAM variability may also feedback  
81 to force climate changes through modulating CO<sub>2</sub> outgassing from the Southern Ocean (Saunders et al., 2018)  
82 and Antarctic sea ice extent (Crosta et al., 2021). During the last millennium, a minimum in the SAM index (i.e.,  
83 negative SAM) occurred during the 1400s and a positive trend in the SAM (with superimposed interannual to  
84 century-scale variability) is evident since this time (Fig. 1a). Anthropogenic forcing of the positive SAM trend since  
85 the mid-20th Century has now moved the mean state of the SAM to its most positive state over at least the last  
86 1000 years (Abram et al., 2014).

87 Climate simulations of the SAM response to rising atmospheric greenhouse gas levels and stratospheric  
88 ozone depletion over the last century compare reasonably well to observations and proxy data (Miller et al., 2006;  
89 Raphael and Holland, 2006; Swart and Fyfe, 2012; Gillett and Fyfe, 2013; Zheng et al., 2013). However, further  
90 back in time, models are unable to reproduce the structure or magnitude of pre-industrial SAM trends that are  
91 reconstructed from proxies (Abram et al., 2014). This could be due to errors in the reconstructions, or a  
92 systematic issue in the way the SAM is forced or represented in current climate models (Abram et al., 2014;  
93 Gillett and Fyfe, 2013). Visually, the temporal evolution of the reconstructed SAM over the last millennium  
94 resembles some of the characteristics of long-term changes in solar irradiance over this time (Fig. 1a–c).  
95 Variations in the solar constant (i.e., the rate at which energy reaches the Earth's surface from the sun) have  
96 previously been suggested as an important driver of the SAM on observational time scales (Kuroda et al., 2007;  
97 Kuroda and Kodera, 2005; Kuroda and Shibata, 2006; Roscoe and Haigh, 2007; Lu et al., 2011). The solar  
98 constant varies naturally in an 11-year solar cycle, and recent work using changes in radiocarbon (<sup>14</sup>C) from  
99 annually resolved and accurately dated tree rings confirms that the 11-yr cycle was present throughout the last  
100 millennium (Brehm et al., 2021) (Fig. 1d). Other proxies (e.g., cosmogenic isotopes such as beryllium-10, <sup>10</sup>Be)  
101 also indicate that longer-term trends in solar forcing also occur on century and millennial scales (Steinhilber et al.,  
102 2009; Gray et al., 2010). During the last millennium, solar modulation reached a minimum during the Spörer  
103 (1388–1558) and Maunder (1621–1718) Grand Solar Minima events. While the temporal history of changes in  
104 solar forcing during the last millennium are well known, there are different published magnitudes for solar  
105 irradiance changes (Fig. 1b). Existing last millennium climate simulations have almost exclusively been run using  
106 the low amplitude solar forcing scenarios (e.g., Steinhilber et al., 2009) and in model set ups that do not  
107 accommodate solar-relevant atmospheric chemistry or wavelength specification. This raises the possibility that  
108 the effects of solar forcing may not have been adequately included in last millennium simulations, potentially  
109 accounting for data-model SAM discrepancies.

110 Here we explore the sensitivity of the SAM to variations in solar forcing, in an attempt to understand if  
111 variations in solar irradiance may have affected SAM variability over the last millennium (Fig. 1). We explore  
112 simulations with constant solar forcing values that correspond to the range of total solar irradiance values from



113 the high amplitude solar reconstruction of Shapiro et al. (2011), as well as additional extreme solar forcing values.  
114 In addition, we investigate transient simulations for the last millennium using intermediate and high amplitude  
115 solar forcing scenarios that complement existing low amplitude transient solar forcing experiments. Our findings  
116 demonstrate that the mean state of the SAM can be significantly altered by changes in solar irradiance, and that  
117 transient solar forcing of a magnitude equivalent to high amplitude scenarios for the last millennium are sufficient  
118 for a significant solar effect on the SAM to become evident despite the large magnitude of internal SAM  
119 variability. Last millennium simulations using high amplitude solar forcing show an improved agreement with  
120 proxy-based SAM reconstructions, suggesting that the effects of solar forcing may not be adequately  
121 represented in current last millennium climate model simulations.

122

123

## 124 **2 Methods**

### 125 **2.1 Reconstructions**

126 The last millennium reconstructions that we use in this study are for the annual mean SAM index. These  
127 are based on (i) a multiproxy network spanning Antarctica and South America where the temperature anomalies  
128 caused by SAM variations are strong (Abram et al., 2014), and (ii) an extensive network of proxies from across the  
129 Southern Hemisphere, using a long calibration period and a correlation plus stationarity criterion for proxy  
130 selection (Dätwyler et al., 2018). Hereafter, these SAM reconstructions are referred to as A14 (Abram et al., 2014)  
131 and D18 (Dätwyler et al., 2018). The A14 and D18 reconstructions share similar features in their long-term trends  
132 (Fig. 1a), despite potential regional biases in the proxy networks used for the reconstructions and uncertainty  
133 related to non-stationary proxy-SAM relationships (Huiskamp and McGregor, 2021; Hessler et al., 2017). Both  
134 reconstructions indicate that the most negative phase of SAM conditions occurred during the 1400s prior to a  
135 progressive, multi-century positive trend in the SAM since the 1400s including the rapid 20th Century increase in  
136 the SAM. Both reconstructions also record strong interannual to centennial variability on top of these long-term  
137 trends, with this characteristic particularly evident in the A14 reconstruction.

138 The A14 and D18 reconstructions were both developed using the instrumental SAM index as a  
139 calibration target (i.e., Marshall, 2003, and Fogt et al., 2009, respectively); however, the A14 reconstruction  
140 displays a larger magnitude of variability (Fig. 1a). This difference in magnitude is due to differences in the way  
141 the annual SAM index can be calculated from instrumental data (Fig. 2). For example, the instrumental SAM index  
142 (Marshall, 2003; <http://www.nerc-bas.ac.uk/icd/gjma/sam.html>) is publicly available in both monthly and annual  
143 resolutions. Here, the annual resolution SAM index is calculated directly using the differences of annual means of  
144 mean sea level pressure (MSLP) data at 40°S and 65°S. Alternatively, the monthly resolution SAM data  
145 (calculated from differences of monthly means of MSLP data at 40°S and 65°S) can be used to then calculate  
146 annual averages of the SAM. The two approaches result in similar trends and interannual variability of the SAM;  
147 however, the magnitude of the directly calculated annual SAM index is 2.7-times larger than the annual mean  
148 SAM derived from the monthly SAM index (Fig. 2).





149           The A14 and D18 SAM reconstructions both use an annual SAM index as their calibration target, but A14  
150 used a calibration annual mean SAM index calculated from annual data (i.e., red line in Fig. 2), while D18 used a  
151 calibration annual mean SAM index calculated from monthly data (e.g., orange line in Fig. 2). Consequently, while  
152 the two reconstructions produce similar patterns and trends of annual SAM variability during the last millennium,  
153 they have markedly different magnitudes of change due to differences in the instrumental calibration data used  
154 (Fig. 3a). To confirm this, we recalculate the A14 reconstruction using the alternate calibration target (i.e.,  
155 calibrated to the annual SAM index derived from monthly SAM data, as in the D18 reconstruction). This rescaled  
156 reconstruction (referred to hereafter as A14-rescaled) has interannual to centennial variability and trends in the  
157 last millennium that are of similar magnitude as the D18 reconstruction (Fig. 3b), confirming that the source of  
158 apparent discrepancy between the A14 and D18 reconstructions is primarily due to the different instrumental  
159 targets used to calibrate the reconstructions.

160           In this study we use the A14, D18 and A14-rescaled SAM reconstructions as indicators of temporal  
161 changes in the mean state of SAM during the last millennium. These are used in data–model comparisons to  
162 determine if different solar-forced model simulations are able to reproduce characteristics of reconstructed SAM  
163 changes during the last millennium.

164

## 165 **2.2 Model Simulations**

166           The model simulations in this study were performed using the Commonwealth Scientific and Industrial Research  
167 Organisation Mark 3L (CSIRO Mk3L) coupled climate system model, version 1.2 ( Phipps et al., 2011, 2012,  
168 2013). CSIRO Mk3L is a fully coupled general circulation model that includes components describing the  
169 atmosphere, ocean, sea ice, and land surface. The horizontal resolution of the atmosphere, sea ice, and land  
170 surface models is  $5.6^\circ \times 3.2^\circ$  in the longitudinal and latitudinal dimensions, respectively, with 18 vertical levels.  
171 The horizontal resolution of the ocean model is  $2.8^\circ \times 1.6^\circ$ , with 21 vertical levels. CSIRO Mk3L was used within  
172 this study as it is computationally efficient, allowing for many multi-century to millennia-scale experiments to be  
173 performed.

174           We investigate how the SAM changes in a series of ‘solar constant’ experiments and transient  
175 experiments. Specifically, we perform:

176           (a) Seven solar constant experiments, where the solar constant (i.e., Total Solar Irradiance [TSI], with no  
177 wavelength dependence) was changed to capture the range of proxy-based realistic solar values in the Shapiro  
178 reconstruction ( $-7$ ,  $-3$ ,  $+1$  and  $+3 \text{ W m}^{-2}$  anomalies relative to a  $1365 \text{ W m}^{-2}$  control), as well as unrealistic  
179 extreme solar forcings (e.g.,  $-15$ ,  $+7$  and  $+35 \text{ W m}^{-2}$  anomalies) to test the response of the model (Fig. 1c). These  
180 experiments use preindustrial  $\text{CO}_2$  (280 ppm) and we run each experiment to equilibrium. In our analysis of the  
181 model output we primarily focus on the transient response of the SAM to the changed solar constant within the  
182 first 200 years of each run (Fig. 4), where the climate has not yet equilibrated to the new solar forcing. These  
183 experiments are referred to using their solar constant anomaly value (e.g., S-7, S+3, etc.)

184           (b) Three-member ensembles of transient experiments using three solar forcing scenarios for the last  
185 millennium. These transient experiments were initialised from the control used in Phipps et al. (2013) (refer to



186 (Phipps et al., 2013) for further details), and all include orbital, greenhouse gas, and solar forcings. The first  
187 ensemble is the orbital-greenhouse gases-solar ('OGS') ensemble first published in Phipps et al. (2013), which  
188 uses the Steinhilber et al. (2009) solar forcing. We build upon this 'OGS' ensemble by performing additional  
189 experiments with modified solar forcing (Fig. 1b). The second ensemble of transient experiments uses an  
190 amplified Steinhilber et al. (2009) forcing, where the magnitude of the transient solar forcing anomaly relative to  
191 the long-term mean is doubled (hereafter referred to as 'OGS-x2'). The third ensemble of transient experiments  
192 uses the Shapiro et al. (2011) high amplitude solar forcing that was included as a last millennium forcing option in  
193 the Paleoclimate Model Intercomparison Project, phase 3 (PMIP3) (Schmidt et al., 2012) and is hereafter referred  
194 to as 'OGS-Shapiro'. The CSIRO Mk3L model does not include interactive chemistry, nor do we prescribe ozone  
195 variations scaled to the solar forcing in our experiments in an attempt to replicate the response of atmospheric  
196 chemistry during the last millennium. Each experiment was run for 1–2000 CE. Here, we focus our analysis to  
197 850–1900 CE, to avoid the influence of strong anthropogenic greenhouse gas forcings after 1900.

198 We supplement our transient experiments with CSIRO Mk3L using previously published simulations  
199 using the HadCM3 model ('Euroclim500'; Schurer et al., 2014). These simulations include one full-forcing  
200 ensemble member for 800–2000 CE, three full-forcing ensemble members for 1400–2000 CE, four 'weak solar'  
201 only ensemble members for 1400–2000 CE, and one 'solar Shapiro' only run for 800–2000 CE using the solar  
202 reconstruction from Shapiro et al. (2011). Forcings used in the HadCM3 experiments follow the PMIP3 protocol  
203 (Schmidt et al., 2011; Schmidt et al., 2012); specifically, the solar reconstruction used in the full-forcing and  
204 'weak solar' runs is based on a combination of Steinhilber et al. (2009) (for times prior to 1810) and Wang et al.  
205 (2005) (for 1810–2000) (see Schurer et al., 2014, for further details).

206 The SAM index was calculated for each model run following the definition from Gong and Wang (1999):  
207  $SAM = P^*_{40^{\circ}S} - P^*_{65^{\circ}S}$ , where  $P^*$  is the normalised annual zonal mean MSLP anomaly in the model relative to  
208 climatology. For the solar constant experiments, we use the solar constant ( $1365 \text{ W m}^{-2}$ ) control run as our  
209 climatology. This allows us to assess the effect of modifying the solar constant anomaly on the SAM mean state  
210 in the other solar constant experiment relative to the  $1365 \text{ W m}^{-2}$  control. In the transient experiments we use the  
211 1900–1999 period as our climatology to assess pre-industrial changes in the SAM mean state over the last  
212 millennium.

213

214

### 215 **3 Results**

#### 216 **3.1 Solar constant experiments**

217 The solar constant experiments demonstrate how changes in the intensity of solar forcing influence the SAM  
218 mean and extreme states (Fig. 5, Fig. 6). The distribution of the mean annual SAM index is significantly different  
219 from the control in the S–15, S–7, and S+35 experiments (based on Welch's  $t$ -test,  $P < 0.05$ , see Fig. 5a). In  
220 particular, changing the solar constant results in a mean shift in the SAM but no significant difference in the  
221 magnitude of SAM variability about this mean shift (using a Kolmogorov–Smirnov test,  $P > 0.05$ ) (Fig. 5a). This  
222 mean shift in the SAM results in a change in the number of extreme events (outside  $\pm 2\sigma$  of the control run),



223 whereby a reduced solar forcing (i.e., S-15, S-7, and S-3) results in an increase in extreme negative SAM events  
224 and decrease in extreme positive SAM events, and vice versa for the increased solar forcing experiments (Fig.  
225 5b).

226 The spatial patterns of anomalies in the solar constant experiments demonstrate the consistent  
227 influences that changes in solar intensity have on the SAM and Southern Hemisphere climate (Fig. 5c-h).  
228 Negative solar forcing anomalies result in a decrease in MSLP over the Southern Hemisphere mid-latitudes and  
229 an increase in MSLP over the Antarctic, and thus a reduced meridional pressure gradient between these zones  
230 (Fig. 5c, f-g). This is associated with an enhancement of the surface temperature gradient between the mid-  
231 latitudes and Antarctica (Fig. 5d; i.e., Antarctica cools more than the mid-latitudes) and decreased westerly wind  
232 anomalies in the Southern Ocean jet (Fig. 5e), leading to a mean negative shift in the SAM index and an increase  
233 in the number of extreme negative SAM events relative to extreme positive events. The opposite is also true with  
234 positive solar forcing, which leads to increased MSLP over the mid-latitudes, decreased MSLP over Antarctica,  
235 and consequently strengthens the meridional pressure gradient and the westerly wind jet. This results in a more  
236 positive mean SAM with an increase in the frequency of extreme positive SAM events. We note that there is an  
237 asymmetry in the effect of changing the solar constant, with a larger response seen in the negative solar constant  
238 experiments (i.e., S-3, S-7) than the positive solar constant anomalies (i.e., S+3, S+7) (Fig. 5a-e). The solar  
239 constant experiments also show that the magnitude of MSLP change over the Antarctic (65°S) is larger than over  
240 the mid-latitudes (40°S) in response to changes in solar forcing (Fig. 5c).

241

### 242 3.2 Transient experiments for the last millennium

243 The transient simulations build upon our findings from the solar constant experiments by modelling the time  
244 evolution of the SAM index during the last millennium based on different amplitudes of transient solar forcing (Fig.  
245 7). The simulations also include transient orbital and greenhouse gas forcing, and so we express the results using  
246 radiative forcing (instead of solar irradiance) and focus on pre-industrial times (i.e., prior to 1900). The ensemble  
247 mean SAM index from the low solar amplitude OGS experiments (Phipps et al., 2013) is not significantly  
248 correlated with the radiative forcing. This indicates that the low amplitude solar forcing in these simulations is not  
249 large enough to modulate the mean SAM state in a way that is detectable beyond the magnitude of unforced  
250 internal SAM variability. However, the ensemble mean SAM index from the intermediate solar amplitude OGS-x2  
251 experiments is positively correlated with radiative forcing for pre-industrial times ( $r = 0.43$ ,  $P < 0.05$ , effective  
252 sample size  $N_{eff} = 15.8$ ; based on 70-yr moving averages stepped by 35 years, with effective sample size taking  
253 into account lag-1 autocorrelation of the time series; Fig. 7a-b). However, for individual ensemble members with  
254 intermediate amplitude solar forcing, we cannot reject the null hypothesis that there is no correlation.

255 In contrast, the SAM index for the high amplitude OGS-Shapiro simulations is significantly correlated  
256 with the radiative forcing anomaly (Fig. 7c). The correlation coefficient between radiative forcing and the SAM  
257 index in the ensemble mean is 0.64 ( $P < 0.05$ ,  $N_{eff} = 14.4$ ) for pre-industrial times (i.e., 850-1900). Each of the  
258 individual ensemble members in the high amplitude solar experiments also displays a significant long-term SAM-



259 radiative forcing relationship over the last millennium, demonstrating a forced signal detectable beyond the large  
260 range of internal SAM variability.

261 We explore this relationship further by binning the model results across all of the transient experiments  
262 based on the magnitude of radiative forcing (Fig. 8). Increasingly negative radiative forcing anomalies result in an  
263 increasingly negative SAM index (Fig. 8a–b). Binning across all ensemble members based on radiative forcing  
264 anomalies further illustrates the linear relationship between reduced radiative forcing and a more negative mean  
265 SAM (Fig. 8b). The zonal mean MSLP and temperature profiles (Fig. 8c–d) and spatial structure of MSLP  
266 anomalies (Fig. 8e–h) are consistent with the anomalies produced in the solar constant experiments (Fig. 5). This  
267 suggests a consistent response of mid to high-latitude Southern Hemisphere climate to changes in solar forcing  
268 within the CSIRO Mk3L experiments, that is also robust across different experiment designs.

269 Overall, our experiments show that a decrease in solar radiative forcing (in both the constant solar and  
270 transient solar forcing runs) results in a mean negative SAM shift. Reducing solar forcing by  $1.5\text{--}1.0\text{ W m}^{-2}$  is  
271 roughly equivalent to a  $\sim 7\text{ W m}^{-2}$  reduction in the solar constant (based on scaling the change in TSI by 0.7/4;  
272 Lean and Rind, 1998). Both the S–7 fixed solar constant experiment and high amplitude transient radiative  
273 forcing of  $-1.5$  to  $-1.0\text{ W m}^{-2}$  result in a statistically significant negative anomaly in the SAM that is detectable  
274 despite the large magnitude of unforced internal variability of the SAM. These simulation results with the CSIRO  
275 Mk3L model suggest that reconstructed negative SAM conditions during the last millennium could have been the  
276 result of reduced solar forcing at this time.

277

278

#### 279 **4 Comparison with reconstructions**

280 Previous work using low amplitude solar forcing experiments has not found any significant relationship between  
281 solar forcing and reconstructed long-term changes in the annual SAM during the last millennium (Abram et al.,  
282 2014; Dätwyler et al., 2018). However, extreme changes in solar forcing in our model experiments that are  
283 comparable with high amplitude estimates of solar irradiance anomalies during the last millennium (Shapiro et al.,  
284 2011) are able to produce a significant change in the mean SAM index, where a  $-7\text{ W m}^{-2}$  change in solar  
285 irradiance (or a roughly  $-1.23\text{ W m}^{-2}$  change in radiative forcing) results in a significant negative shift in the mean  
286 SAM index. To explore further whether solar forcing may help to explain reconstructed trends in the SAM during  
287 the last millennium, we compare our model results with proxy-based SAM reconstructions (see Section 2.1).

288 To test the significance of changes in the SAM during the last millennium, we use each of the SAM  
289 reconstructions to assess whether 70-yr sliding windows of the annual SAM reconstructions are significantly  
290 ( $P < 0.05$ ; Wilcoxon rank-sum test) more negative than a 70-yr reference window of the reconstruction between  
291 1831–1900. This reference interval was chosen as it is prior to strong positive SAM trends caused by  
292 anthropogenic forcing during the 20th Century, and is longer than the standard 50-year preindustrial period so as  
293 to improve the robustness of the distribution testing. These tests show that across all three reconstructions the  
294 SAM index was significantly more negative between approximately 1390 and 1715 CE compared with the 1831–



295 1900 reference interval (Fig. 9). The A14 and A14-rescaled reconstructions also indicate significant negative SAM  
296 distributions prior to around 1140 CE (Fig. 9).

297 Carrying out the same distribution tests on the CSIRO Mk3L transient simulations (Fig. 10) shows that  
298 there are no significant negative shifts of the SAM index during the last millennium in the OGS ensemble mean  
299 with low amplitude solar forcing. By comparison, the OGS-Shapiro ensemble mean shows a strong and  
300 sustained negative SAM shift that peaked at approximately 1460 CE. This is in good agreement with the interval  
301 where all SAM reconstructions also display a significant negative shift in the SAM. The OGS-Shapiro ensemble  
302 mean also shows earlier intervals where the SAM index is significantly more negative than the 1831–1900  
303 reference interval. Exact matches in the start and end times of significant negative shifts caused by solar forcing  
304 in the SAM simulations and reconstructions are not expected due to the additional effect of large unforced  
305 internal variability in the SAM (i.e., as seen in differences between ensemble members runs with the same solar  
306 forcing). However, we do find that the maximum significance in negative SAM distribution shifts in the OGS-  
307 Shapiro ensemble mean is around 1460 CE (Fig. 10d), which matches the timing of maximum significant shifts in  
308 all of the last millennium SAM reconstructions (Fig. 9d; approximately 1415–1560 CE). We also find a strongly  
309 significant negative shift in the simulated SAM index peaking at around 1025 CE (Fig. 10d), which coincides with  
310 the reconstructed significant shift in the A14 and A14-rescaled reconstructions prior to 1140 CE (Fig. 9).

311 Direct correlation of the reconstructions and transient simulations further shows that the A14 proxy-  
312 based SAM reconstruction shares significant ( $P < 0.05$ ) variance during the pre-industrial last millennium (1000–  
313 1900 CE) with the ensemble mean SAM index of the transient solar scenario simulations run with CSIRO Mk3L  
314 (Fig. 11a). The increasing strength of the correlations with increasing magnitude of solar forcing indicates  
315 improved coherence between the multi-decadal variability and long-term trends of the reconstructed and  
316 modelled SAM when strong solar forcing is used over the last millennium. There are differences in the shorter-  
317 term details of the modelled and reconstructed SAM indices, such as the timing during the 1400s when the most  
318 negative SAM conditions are reached. However, these differences are of a comparable magnitude to the internal  
319 variability between ensemble members of the same experiment (Fig. 7) and so may simply represent differences  
320 between realisations (including the reconstructed single real-world realisation) in unforced variability of the SAM  
321 on top of the solar-forced variability and trends.

322 The D18 SAM reconstruction during the pre-industrial last millennium is not significantly correlated with  
323 the ensemble mean SAM index of any of the CSIRO Mk3L transient solar forcing experiments (Fig. 12a). This  
324 appears to be mostly related to differences between the modelled and reconstructed SAM indices prior to 1400.  
325 This also corresponds to an apparent increase in the magnitude of noise within the D18 reconstruction prior to  
326 1400 (Fig. 9c), and a reduction of reconstruction skill (negative reduction of error [RE]) for the D18 reconstruction  
327 prior to 1400 (Dätwyler et al., 2018), and may reflect reduced reconstruction fidelity due to the sparse proxy  
328 network during the early stages of the last millennium. Visually, the maximum negative SAM anomaly during the  
329 1400s and the long-term positive trend since that time appears to correspond well between the transient  
330 simulations and the D18 reconstruction, particularly for the strong amplitude solar forcing experiments (Fig. 12a).

331



## 332 5 Discussion

333 There have so far been few studies exploring the influence of high amplitude changes in solar forcing during the  
334 last millennium. Research by Schurer et al. (2014) found little influence of stronger solar variability on Northern  
335 Hemisphere temperature reconstructions of the last millennium using the HadCM3 model. However, a  
336 comparison of the Shapiro et al. (2011)-solar forced run in HadCM3 (Schurer et al., 2014) and our OGS-Shapiro  
337 simulation show some similarities in the long-term trends of the SAM index (Fig. 11). In particular, both CSIRO  
338 Mk3L and HadCM3 show a large negative excursion in the SAM index around 1450 CE in their strong solar  
339 forcing simulations (Fig. 11, purple and red time series in Fig. 11a and 11b, respectively). The transient strong-  
340 solar forcing simulation from HadCM3 has a significant ( $P < 0.05$ ) correlation with both proxy-based SAM  
341 reconstructions ( $r = 0.48$  for A14, and  $r = 0.73$  for D18). In contrast, last millennium correlations are not significant  
342 for the SAM reconstructions with the ensemble mean SAM index in the HadCM3 weak-solar forcing only  
343 simulation and full-forcing (including weak-solar forcing) simulations (Fig. 11b, Fig. 12b). The HadCM3 strong  
344 solar forcing experiment thus corroborates our findings using CSIRO Mk3L, indicating that high amplitude solar  
345 forcing of last millennium simulations has a detectable effect on the annual SAM that improves the agreement  
346 between modelled realisations of the SAM index and proxy-based SAM reconstructions.

347 Solar activity is thought to influence climate, the SAM, and its Northern Hemisphere equivalent—the  
348 Northern Annular Mode (NAM)—through either ‘top-down’ (e.g., via changes associated with stratospheric-  
349 tropospheric coupling due to ozone and UV-related stratospheric temperature and wind variations; Gray et al.,  
350 2010) or ‘bottom-up’ mechanisms (e.g., through associated changes in sea surface temperature [SST] and ocean  
351 heat uptake; Gray et al., 2010; Meehl et al., 2008). Notably, resolving the former mechanism requires climate  
352 model simulations using interactive stratospheric chemistry that are computationally expensive to run (and not  
353 currently feasible for the last millennium), while ‘bottom-up’ drivers do not require a well-resolved stratosphere or  
354 changes in stratospheric ozone (Meehl et al., 2008). Studies based on observations and/or chemistry-enabled  
355 climate models have previously suggested that the SAM (and the NAM) is sensitive to changes in solar activity  
356 associated with the 11-year solar cycle (Kuroda et al., 2007; Kuroda and Kodera, 2005; Kuroda and Shibata,  
357 2006; Gray et al., 2010; Gray et al., 2013; Ma et al., 2018; Kuroda, 2018; Arblaster and Meehl, 2006). These  
358 studies link variations in the SAM/NAM to changes in stratospheric temperatures and/or stratospheric-  
359 tropospheric coupling. For example, during years of higher solar activity, there is a stratospheric extension of the  
360 SAM signal (Kuroda and Kodera, 2005), related to a corresponding increase in stratospheric-tropospheric  
361 coupling (Kuroda et al., 2007). A similar process is seen for the NAM, though there may be a 2–4 year lagged  
362 response of positive NAM following a solar high (Gray et al., 2013; Ma et al., 2018). Solar activity incites variations  
363 in stratospheric temperature and winds related to changes in UV irradiance and ozone production, while  
364 associated variations in stratospheric-tropospheric coupling result in changes in surface climate (e.g., a ‘top-  
365 down’ forcing) (Gray et al., 2010). This varies from proposed ‘bottom-up’ mechanisms for solar variations  
366 influencing surface climate, which involve changes in SST and ocean heat uptake during periods of increased  
367 solar activity, resulting in an increase in latent heat flux and evaporation, which ultimately leads to intensified  
368 precipitation along convergence zones and stronger trade winds (Meehl et al., 2008; Meehl et al., 2003; Gray et



369 al., 2010), as well as less heating over the ocean than land (Meehl et al., 2003). Solar forcing may also influence  
370 climate through a combination of both top-down and bottom-up mechanisms (Rind et al., 2008), and simulations  
371 with both mechanisms working together result in a stronger tropical SST response more similar to observations  
372 than simulations with only a single mechanism (Meehl et al., 2009).

373 As the models examined in this study do not have a well-resolved stratosphere or incorporate interactive  
374 stratospheric ozone, we suggest our simulated changes in the SAM are caused by a ‘bottom-up’ mechanism. We  
375 find comparable changes in our increased solar constant experiments to previous studies invoking a bottom-up  
376 mechanism, such as an increase in equatorial evaporation and precipitation, as well as a greater increase in land  
377 surface temperatures than over the ocean (Fig. 6). Within the atmosphere, our experiments show an increase in  
378 solar forcing causes an increase in temperature throughout the tropics, with a larger increase in the upper  
379 troposphere than surface, as well as cooling in the high-latitude upper troposphere and a reduced warming in the  
380 lower troposphere along 40°–60°S (Fig. 13b). This increase in temperature is combined with a westerly wind  
381 anomaly that spans from the tropical upper troposphere to the high latitudes (~50°S) and extends into the lower  
382 troposphere (Fig. 13a)—all of which are similar to the climate effects simulated from an increase in radiative  
383 forcing by greenhouse gases (e.g., Kushner et al., 2001; Lim and Simmonds, 2009; Butler et al., 2011). The  
384 poleward contraction in the westerly jets around 55°S is particularly pronounced in the S+7 and S+35 scenarios,  
385 as is the increased meridional temperature gradient (e.g., tropics warming faster than the Southern Ocean),  
386 leading to the development of a mean positive SAM state. A decrease in solar forcing results in an approximately  
387 inverse pattern, with cooling in the tropical upper troposphere, warming in the high-latitude upper troposphere,  
388 and more cooling in the tropical lower troposphere, with minimal cooling in the high latitudes (Fig. 13b), as well as  
389 a decrease in the zonal wind anomaly across the tropical–high latitude upper troposphere and into the high  
390 latitude lower troposphere (Fig. 13). Overall, this indicates a weakening of the westerly jet (i.e., negative zonal  
391 wind anomaly around ~50°S). Solar forcing is primarily shortwave and varies seasonally and spatially, with  
392 greater influence in the tropics, while greenhouse gas forcing is more spatially uniform (Meehl et al., 2003). While  
393 solar forcing affects climate differently to greenhouse gas forcing, it is possible that we find in our solar  
394 experiments a broadly similar tropospheric response as expected from greenhouse gases due to the extremely  
395 large magnitude changes in our solar forcing experiments combined with exploring transient mean state changes  
396 over only the first 200 years (Fig. 4) of the solar constant experiments.

397 Overall, our findings do suggest that the effects of solar forcing on the SAM are not adequately  
398 represented in current last millennium climate simulations. It is possible that the reconstructed minimum in the  
399 SAM during the 15th Century was a response to a minimum in solar irradiance at this time, and that this solar  
400 response is not reproduced in last millennium simulations that are forced with low amplitude solar forcing.  
401 However, our results do not necessarily imply that solar forcing of the last millennium involved the large  
402 amplitude changes of the Shapiro et al. (2011) forcing scenario. The large amplitude solar forcing used in our  
403 transient experiments is a plausible forcing scenario provided as an option for last millennium experiment design  
404 of the Coupled Model Intercomparison Project (Schmidt et al., 2012). But this strong solar forcing scenario (i.e.,  
405 Shapiro et al., 2011) has rarely been applied in last millennium simulations and it has been argued that the





406 Shapiro et al. (2011) TSI changes are overestimated by about a factor of two, due to the model used in their  
407 methodology (Judge et al., 2012). Instead, it may be that in climate models that do not have the interactive  
408 atmospheric chemistry needed to permit solar-impacts on stratospheric ozone, a large amplitude of solar forcing  
409 is instead needed to reproduce the last millennium climate impacts on the SAM that were caused by more  
410 modest solar forcing changes. While we cannot rule out the possibility that the strength of the forcing allows our  
411 experiments to reproduce changes in the SAM without a realistic representation of all the forcings involved, our  
412 strong solar forcing experiments produce a SAM response that better replicates reconstructed changes in the  
413 SAM during the last millennium.

414

415

## 416 **6 Conclusion**

417 Palaeoclimate reconstructions indicate large changes in the SAM during pre-industrial times that are not  
418 replicated in current last millennium climate simulations. We explore changes in solar forcing on the SAM using  
419 solar constant and last millennium transient simulations that cover large amplitude solar changes and find that  
420 the SAM index significantly decreases (increases) with a decrease (increase) in solar forcing. The magnitude of  
421 solar forcing change required for a significant change in the SAM index is much greater than the most commonly  
422 used solar forcing scenarios for the last millennium, with an approximately  $7 \text{ W m}^{-2}$  decrease in total solar  
423 irradiance (or  $1.5 \text{ W m}^{-2}$  decrease in radiative forcing) required before the effect of solar forcing on the SAM can  
424 be distinguished from the large range of unforced SAM variability. Transient simulations of the last millennium  
425 with strong solar forcing result in an improved and significant agreement with proxy-based reconstructions of the  
426 SAM. It is plausible that solar forcing may have been an important driver in long-term SAM trends prior to the  
427 strong anthropogenic forcing of the 20th and 21st centuries, and that current climate model simulations of the  
428 last millennium do not adequately represent the effect of solar variability on mid to high latitude Southern  
429 Hemisphere climate. This may be due to a higher magnitude of solar irradiance changes than is usually applied in  
430 last millennium simulations, or (more likely) due to the absence of important physical and chemical processes in  
431 coupled global climate models that would allow more moderate changes in solar forcing to have a discernible  
432 impact on high latitude climate.

433



434 **7 Acknowledgements**

435 We thank the Australian Research Council for support of this research through the Centre of Excellence for  
436 Climate Extremes (CE170100023)), Discovery Project (DP140102059), Future Fellowship (FT160100029) and the  
437 Australian Centre for Excellence in Antarctic Science (SR200100008). This work was also supported by the  
438 Climate Systems Hub of the Australian Government's National Environmental Science Program, and was made  
439 possible by computational resources provided by the Australian Government through the National Computational  
440 Infrastructure, including a grant (xf4) through the ANU merit allocation scheme.

441

442

443 **8 Author contributions**

444 N.J.A. devised the study. C.E.K. performed the solar constant experiments, and N.M.W. and S.J.P. performed the  
445 transient simulations. N.M.W. and N.J.A. performed the data analyses with help from G.B., and N.M.W. made the  
446 figures. N.M.W. wrote the manuscript, with contributions from all co-authors.

447

448

449 **9 Competing interests**

450 The authors declare no competing interests.

451

452

453 **10 Code/Data availability**

454 Code and data will be archived in a public repository upon acceptance.



455 **References**

- 456 Abram, N. J., Mulvaney, R., Vimeux, F., Phipps, S. J., Turner, J., and England, M. H.: Evolution of the Southern  
457 Annular Mode during the past millennium, *Nature Climate Change*, 4, 564-569, 2014.
- 458 Arblaster, J. M. and Meehl, G. A.: Contributions of external forcings to southern annular mode trends, *Journal of*  
459 *climate*, 19, 2896-2905, 2006.
- 460 Arblaster, J. M., Meehl, G. A., and Karoly, D. J.: Future climate change in the Southern Hemisphere: Competing  
461 effects of ozone and greenhouse gases, *Geophysical Research Letters*, 38, 2011.
- 462 Banerjee, A., Fyfe, J. C., Polvani, L. M., Waugh, D., and Chang, K.-L.: A pause in Southern Hemisphere  
463 circulation trends due to the Montreal Protocol, *Nature*, 579, 544-548, 2020.
- 464 Barnes, E. A. and Polvani, L.: Response of the midlatitude jets, and of their variability, to increased greenhouse  
465 gases in the CMIP5 models, *Journal of Climate*, 26, 7117-7135, 2013.
- 466 Brehm, N., Bayliss, A., Christl, M., Synal, H.-A., Adolphi, F., Beer, J., Kromer, B., Muscheler, R., Solanki, S. K.,  
467 and Usoskin, I.: Eleven-year solar cycles over the last millennium revealed by radiocarbon in tree rings,  
468 *Nature Geoscience*, 14, 10–15, 2021.
- 469 Butler, A. H., Thompson, D. W., and Birner, T.: Isentropic slopes, downgradient eddy fluxes, and the extratropical  
470 atmospheric circulation response to tropical tropospheric heating, *Journal of the atmospheric sciences*, 68,  
471 2292-2305, 2011.
- 472 Crosta, X., Etourneau, J., Orme, L.C., Dalaiden, Q., Campagne, P., Swingedouw, D., Goosse, H., Massé, G.,  
473 Miettinen, A., McKay, R.M., Dunbar, R.B., Escutia, C., and Ikehara, M.: Multi-decadal trends in Antarctic  
474 sea-ice extent driven by ENSO–SAM over the last 2,000 years, *Nature Geoscience*, 14, 156–160,  
475 10.1038/s41561-021-00697-1, 2021.
- 476 Dätwyler, C., Neukom, R., Abram, N. J., Gallant, A. J. E., Grosjean, M., Jacques-Coper, M., Karoly, D. J., and  
477 Villalba, R.: Teleconnection stationarity, variability and trends of the Southern Annular Mode (SAM) during  
478 the last millennium, *Climate Dynamics*, 51, 2321-2339, 10.1007/s00382-017-4015-0, 2018.
- 479 Emile-Geay, J., McKay, N. P., Kaufman, D. S., Von Gunten, L., Wang, J., Anchukaitis, K. J., Abram, N. J.,  
480 Addison, J. A., Curran, M. A., and Evans, M. N.: A global multiproxy database for temperature  
481 reconstructions of the Common Era, *Scientific data*, 4, 170088, 2017.
- 482 Fan, K. and Wang, H.: Antarctic oscillation and the dust weather frequency in North China, *Geophysical Research*  
483 *Letters*, 31, 2004.
- 484 Fogt, R. L. and Marshall, G. J.: The Southern Annular Mode: variability, trends, and climate impacts across the  
485 Southern Hemisphere, *Wiley Interdisciplinary Reviews: Climate Change*, e652, 2020.
- 486 Fogt, R. L., Perlwitz, J., Monaghan, A. J., Bromwich, D. H., Jones, J. M., and Marshall, G. J.: Historical SAM  
487 variability. Part II: Twentieth-century variability and trends from reconstructions, observations, and the  
488 IPCC AR4 models, *Journal of Climate*, 22, 5346-5365, 2009.
- 489 Fyfe, J., Boer, G., and Flato, G.: The Arctic and Antarctic Oscillations and their projected changes under global  
490 warming, *Geophysical Research Letters*, 26, 1601-1604, 1999.



- 491 Gillett, N. and Fyfe, J.: Annular mode changes in the CMIP5 simulations, *Geophysical Research Letters*, 40,  
492 1189-1193, 2013.
- 493 Gillett, N. P. and Thompson, D. W.: Simulation of recent Southern Hemisphere climate change, *Science*, 302,  
494 273-275, 2003.
- 495 Gillett, N. P., Kell, T. D., and Jones, P.: Regional climate impacts of the Southern Annular Mode, *Geophysical*  
496 *Research Letters*, 33, 2006.
- 497 Gong, D. and Wang, S.: Definition of Antarctic oscillation index, *Geophysical research letters*, 26, 459-462, 1999.
- 498 Goyal, R., Sen Gupta, A., Jucker, M., and England, M. H.: Historical and projected changes in the Southern  
499 Hemisphere surface westerlies, *Geophysical Research Letters*, 48, e2020GL090849, 2021.
- 500 Gray, L. J., Beer, J., Geller, M., Haigh, J. D., Lockwood, M., Matthes, K., Cubasch, U., Fleitmann, D., Harrison, G.,  
501 and Hood, L.: Solar influences on climate, *Reviews of Geophysics*, 48, 2010.
- 502 Gray, L. J., Scaife, A. A., Mitchell, D. M., Osprey, S., Ineson, S., Hardiman, S., Butchart, N., Knight, J., Sutton, R.,  
503 and Kodera, K.: A lagged response to the 11 year solar cycle in observed winter Atlantic/European weather  
504 patterns, *Journal of Geophysical Research: Atmospheres*, 118, 13,405-413,420, 2013.
- 505 Grise, K. M., Polvani, L. M., Tselioudis, G., Wu, Y., and Zelinka, M. D.: The ozone hole indirect effect: Cloud-  
506 radiative anomalies accompanying the poleward shift of the eddy-driven jet in the Southern Hemisphere,  
507 *Geophysical Research Letters*, 40, 3688-3692, 2013.
- 508 Hendon, H. H., Thompson, D. W., and Wheeler, M. C.: Australian rainfall and surface temperature variations  
509 associated with the Southern Hemisphere annular mode, *Journal of Climate*, 20, 2452-2467, 2007.
- 510 Hessl, A., Allen, K. J., Vance, T., Abram, N. J., & Saunders, K. M.: Reconstructions of the southern annular mode  
511 (SAM) during the last millennium. *Progress in Physical Geography*, 41(6), 834-849. 2017.
- 512 Huiskamp, W. and McGregor, S.: Quantifying Southern Annular Mode paleo-reconstruction skill in a model  
513 framework, *Clim. Past*, 17, 1819-1839, 10.5194/cp-17-1819-2021, 2021.
- 514 Jones, J. M., Fogt, R. L., Widmann, M., Marshall, G. J., Jones, P. D., and Visbeck, M.: Historical SAM variability.  
515 Part I: Century-length seasonal reconstructions, *Journal of Climate*, 22, 5319-5345, 2009.
- 516 Jones, J. M., Gille, S. T., Goosse, H., Abram, N. J., Canziani, P. O., Charman, D. J., Clem, K. R., Crosta, X., de  
517 Lavergne, C., and Eisenman, I.: Assessing recent trends in high-latitude Southern Hemisphere surface  
518 climate, *Nature Climate Change*, 6, 917-926, 2016.
- 519 Judge, P. G., Lockwood, G. W., Radick, R. R., Henry, G. W., Shapiro, A. I., Schmutz, W., and Lindsey, C.:  
520 Confronting a solar irradiance reconstruction with solar and stellar data, *A&A*, 544, A88, 2012.
- 521 Jungclaus, J. H., Bard, E., Baroni, M., Braconnot, P., Cao, J., Chini, L. P., Egorova, T., Evans, M., González-  
522 Rouco, J. F., Goosse, H., Hurrell, G. C., Joos, F., Kaplan, J. O., Khodri, M., Klein Goldewijk, K., Krivova, N.,  
523 LeGrande, A. N., Lorenz, S. J., Luterbacher, J., Man, W., Maycock, A. C., Meinshausen, M., Moberg, A.,  
524 Muscheler, R., Nehrbass-Ahles, C., Otto-Bliesner, B. I., Phipps, S. J., Pongratz, J., Rozanov, E., Schmidt,  
525 G. A., Schmidt, H., Schmutz, W., Schurer, A., Shapiro, A. I., Sigl, M., Smerdon, J. E., Solanki, S. K.,  
526 Timmreck, C., Toohey, M., Usoskin, I. G., Wagner, S., Wu, C. J., Yeo, K. L., Zanchettin, D., Zhang, Q., and  
527 Zorita, E.: The PMIP4 contribution to CMIP6 – Part 3: The last millennium, scientific objective, and



- 528 experimental design for the PMIP4 past1000 simulations, *Geosci. Model Dev.*, 10, 4005-4033,  
529 10.5194/gmd-10-4005-2017, 2017.
- 530 Kuroda, Y.: On the Origin of the Solar Cycle Modulation of the Southern Annular Mode, *Journal of Geophysical*  
531 *Research: Atmospheres*, 123, 1959-1969, 10.1002/2017JD027091, 2018.
- 532 Kuroda, Y. and Kodera, K.: Solar cycle modulation of the Southern Annular Mode, *Geophysical Research Letters*,  
533 32, 10.1029/2005GL022516, 2005.
- 534 Kuroda, Y. and Shibata, K.: Simulation of solar-cycle modulation of the Southern Annular Mode using a  
535 chemistry-climate model, *Geophysical Research Letters*, 33, 10.1029/2005GL025095, 2006.
- 536 Kuroda, Y., Deushi, M., and Shibata, K.: Role of solar activity in the troposphere-stratosphere coupling in the  
537 Southern Hemisphere winter, *Geophysical Research Letters*, 34, 10.1029/2007GL030983, 2007.
- 538 Kushner, P. J., Held, I. M., and Delworth, T. L.: Southern Hemisphere atmospheric circulation response to global  
539 warming, *Journal of Climate*, 14, 2238-2249, 2001.
- 540 Lean, J. and Rind, D.: Climate forcing by changing solar radiation, *J. Climate*, 11, 3069-3094, 10.1175/1520-  
541 0442(1998)011%3C3069%3ACFBCSR%3E2.0.CO;2, 1998.
- 542 Lim, E.-P. and Simmonds, I.: Effect of tropospheric temperature change on the zonal mean circulation and SH  
543 winter extratropical cyclones, *Climate dynamics*, 33, 19-32, 2009.
- 544 Lu, H., Jarvis, M. J., Gray, L. J., and Baldwin, M. P.: High- and low-frequency 11-year solar cycle signatures in  
545 the Southern Hemispheric winter and spring, *Quarterly Journal of the Royal Meteorological Society*, 137,  
546 1641-1656, 10.1002/qj.852, 2011.
- 547 Ma, H., Chen, H., Gray, L., Zhou, L., Li, X., Wang, R., and Zhu, S.: Changing response of the North  
548 Atlantic/European winter climate to the 11 year solar cycle, *Environmental Research Letters*, 13, 034007,  
549 10.1088/1748-9326/aa9e94, 2018.
- 550 Marshall, G. J.: Trends in the Southern Annular Mode from Observations and Reanalyses, *Journal of Climate*, 16,  
551 4134-4143, 10.1175/1520-0442(2003)016<4134:Titsam>2.0.Co;2, 2003.
- 552 Meehl, G. A., Arblaster, J. M., Branstator, G., and van Loon, H.: A Coupled Air–Sea Response Mechanism to  
553 Solar Forcing in the Pacific Region, *Journal of Climate*, 21, 2883-2897, 10.1175/2007jcli1776.1, 2008.
- 554 Meehl, G. A., Arblaster, J. M., Matthes, K., Sassi, F., and van Loon, H.: Amplifying the Pacific climate system  
555 response to a small 11-year solar cycle forcing, *Science*, 325, 1114-1118, 2009.
- 556 Meehl, G. A., Washington, W. M., Wigley, T., Arblaster, J. M., and Dai, A.: Solar and greenhouse gas forcing and  
557 climate response in the twentieth century, *Journal of Climate*, 16, 426-444, 2003.
- 558 Meehl, G. A., Washington, W. M., Arblaster, J. M., Hu, A., Teng, H., Tebaldi, C., Sanderson, B. N., Lamarque, J.-  
559 F., Conley, A., and Strand, W. G.: Climate system response to external forcings and climate change  
560 projections in CCSM4, *Journal of Climate*, 25, 3661-3683, 2012.
- 561 Miller, R. L., Schmidt, G. A., and Shindell, D. T.: Forced annular variations in the 20th century Intergovernmental  
562 Panel on Climate Change Fourth Assessment Report models, *Journal of Geophysical Research:*  
563 *Atmospheres*, 111, 10.1029/2005JD006323, 2006.



- 564 Neukom, R., Schurer, A. P., Steiger, N. J., and Hegerl, G. C.: Possible causes of data model discrepancy in the  
565 temperature history of the last Millennium, *Scientific Reports*, 8, 7572, 10.1038/s41598-018-25862-2,  
566 2018.
- 567 Neukom, R., Barboza, L. A., Erb, M. P., Shi, F., Emile-Geay, J., Evans, M. N., Franke, J., Kaufman, D. S., Lücke,  
568 L., Rehfeld, K., Schurer, A., Zhu, F., Brönnimann, S., Hakim, G. J., Henley, B. J., Ljungqvist, F. C., McKay,  
569 N., Valler, V., von Gunten, L., and Consortium, P. k.: Consistent multidecadal variability in global  
570 temperature reconstructions and simulations over the Common Era, *Nature Geoscience*, 12, 643-649,  
571 10.1038/s41561-019-0400-0, 2019.
- 572 Ortega, P., Lehner, F., Swingedouw, D., Masson-Delmotte, V., Raible, C. C., Casado, M., and Yiou, P.: A model-  
573 tested North Atlantic Oscillation reconstruction for the past millennium, *Nature*, 523, 71-74,  
574 10.1038/nature14518, 2015.
- 575 Otto-Bliesner, B. L., Brady, E. C., Fasullo, J., Jahn, A., Landrum, L., Stevenson, S., Rosenbloom, N., Mai, A., and  
576 Strand, G.: Climate Variability and Change since 850 CE: An Ensemble Approach with the Community  
577 Earth System Model, *Bulletin of the American Meteorological Society*, 97, 735-754, 10.1175/bams-d-14-  
578 00233.1, 2016.
- 579 Phipps, S. J., Rotstayn, L. D., Gordon, H. B., Roberts, J. L., Hirst, A. C., and Budd, W. F.: The CSIRO Mk3L  
580 climate system model version 1.0 – Part 1: Description and evaluation, *Geosci. Model Dev.*, 4, 483-509,  
581 10.5194/gmd-4-483-2011, 2011.
- 582 Phipps, S. J., Rotstayn, L. D., Gordon, H. B., Roberts, J. L., Hirst, A. C., and Budd, W. F.: The CSIRO Mk3L  
583 climate system model version 1.0 – Part 2: Response to external forcings, *Geosci. Model Dev.*, 5, 649-682,  
584 10.5194/gmd-5-649-2012, 2012.
- 585 Phipps, S. J., McGregor, H. V., Gergis, J., Gallant, A. J. E., Neukom, R., Stevenson, S., Ackerley, D., Brown, J. R.,  
586 Fischer, M. J., and van Ommen, T. D.: Paleoclimate Data–Model Comparison and the Role of Climate  
587 Forcings over the Past 1500 Years, *Journal of Climate*, 26, 6915-6936, 10.1175/jcli-d-12-00108.1, 2013.
- 588 Polvani, L. M., Waugh, D. W., Correa, G. J., and Son, S.-W.: Stratospheric ozone depletion: The main driver of  
589 twentieth-century atmospheric circulation changes in the Southern Hemisphere, *Journal of Climate*, 24,  
590 795-812, 2011a.
- 591 Polvani, L. M., Waugh, D. W., Correa, G. J. P., and Son, S.-W.: Stratospheric Ozone Depletion: The Main Driver of  
592 Twentieth-Century Atmospheric Circulation Changes in the Southern Hemisphere, *Journal of Climate*, 24,  
593 795-812, 10.1175/2010jcli3772.1, 2011b.
- 594 Raphael, M. N. and Holland, M. M.: Twentieth century simulation of the southern hemisphere climate in coupled  
595 models. Part 1: large scale circulation variability, *Climate Dynamics*, 26, 217-228, 10.1007/s00382-005-  
596 0082-8, 2006.
- 597 Rind, D., Lean, J., Lerner, J., Lonergan, P., and Leboissier, A.: Exploring the stratospheric/tropospheric  
598 response to solar forcing, *Journal of Geophysical Research: Atmospheres*, 113, 2008.



- 599 Roscoe, H. K. and Haigh, J. D.: Influences of ozone depletion, the solar cycle and the QBO on the Southern  
600 Annular Mode, *Quarterly Journal of the Royal Meteorological Society*, 133, 1855-1864, 10.1002/qj.153,  
601 2007.
- 602 Saunders, K.M., Roberts, S.J., Perren, B. *et al.*: Holocene dynamics of the Southern Hemisphere westerly winds  
603 and possible links to CO<sub>2</sub> outgassing. *Nature Geoscience*, 11, 650–655, 10.1038/s41561-018-0186-5,  
604 2018
- 605 Schmidt, G., Jungclaus, J. H., Ammann, C., Bard, E., Braconnot, P., Crowley, T., Delaygue, G., Joos, F., Krivova,  
606 N., and Muscheler, R.: Climate forcing reconstructions for use in PMIP simulations of the Last Millennium  
607 (v1. 1), *Geoscientific Model Development*, 185-191, 2012.
- 608 Schmidt, G. A., Jungclaus, J. H., Ammann, C., Bard, E., Braconnot, P., Crowley, T., Delaygue, G., Joos, F.,  
609 Krivova, N., and Muscheler, R.: Climate forcing reconstructions for use in PMIP simulations of the last  
610 millennium (v1. 0), 2011.
- 611 Schurer, A. P., Tett, S. F., and Hegerl, G. C.: Small influence of solar variability on climate over the past  
612 millennium, *Nature Geoscience*, 7, 104-108, 2014.
- 613 Sen Gupta, A. and England, M. H.: Coupled ocean–atmosphere–ice response to variations in the southern  
614 annular mode, *Journal of Climate*, 19, 4457-4486, 2006.
- 615 Shapiro, A., Schmutz, W., Rozanov, E., Schoell, M., Haberleiter, M., Shapiro, A., and Nyeki, S.: A new approach  
616 to the long-term reconstruction of the solar irradiance leads to large historical solar forcing, *Astronomy &*  
617 *Astrophysics*, 529, A67, 2011.
- 618 Shindell, D. T. and Schmidt, G. A.: Southern Hemisphere climate response to ozone changes and greenhouse  
619 gas increases, *Geophysical Research Letters*, 31, 2004.
- 620 Son, S. W., Tandon, N. F., Polvani, L. M., and Waugh, D. W.: Ozone hole and Southern Hemisphere climate  
621 change, *Geophysical Research Letters*, 36, 2009.
- 622 Steinhilber, F., Beer, J., and Fröhlich, C.: Total solar irradiance during the Holocene, *Geophysical Research*  
623 *Letters*, 36, 2009.
- 624 Swart, N. and Fyfe, J. C.: Observed and simulated changes in the Southern Hemisphere surface westerly wind-  
625 stress, *Geophysical Research Letters*, 39, 2012.
- 626 Thompson, D. W. and Solomon, S.: Interpretation of recent Southern Hemisphere climate change, *Science*, 296,  
627 895-899, 2002.
- 628 Thompson, D. W. and Wallace, J. M.: Annular modes in the extratropical circulation. Part I: Month-to-month  
629 variability, *Journal of climate*, 13, 1000-1016, 2000.
- 630 Thompson, D. W. J., Solomon, S., Kushner, P. J., England, M. H., Grise, K. M., and Karoly, D. J.: Signatures of  
631 the Antarctic ozone hole in Southern Hemisphere surface climate change, *Nature Geoscience*, 4, 741-749,  
632 10.1038/ngeo1296, 2011.
- 633 Villalba, R., Lara, A., Masiokas, M. H., Urrutia, R., Luckman, B. H., Marshall, G. J., Mundo, I. A., Christie, D. A.,  
634 Cook, E. R., and Neukom, R.: Unusual Southern Hemisphere tree growth patterns induced by changes in  
635 the Southern Annular Mode, *Nature geoscience*, 5, 793-798, 2012.

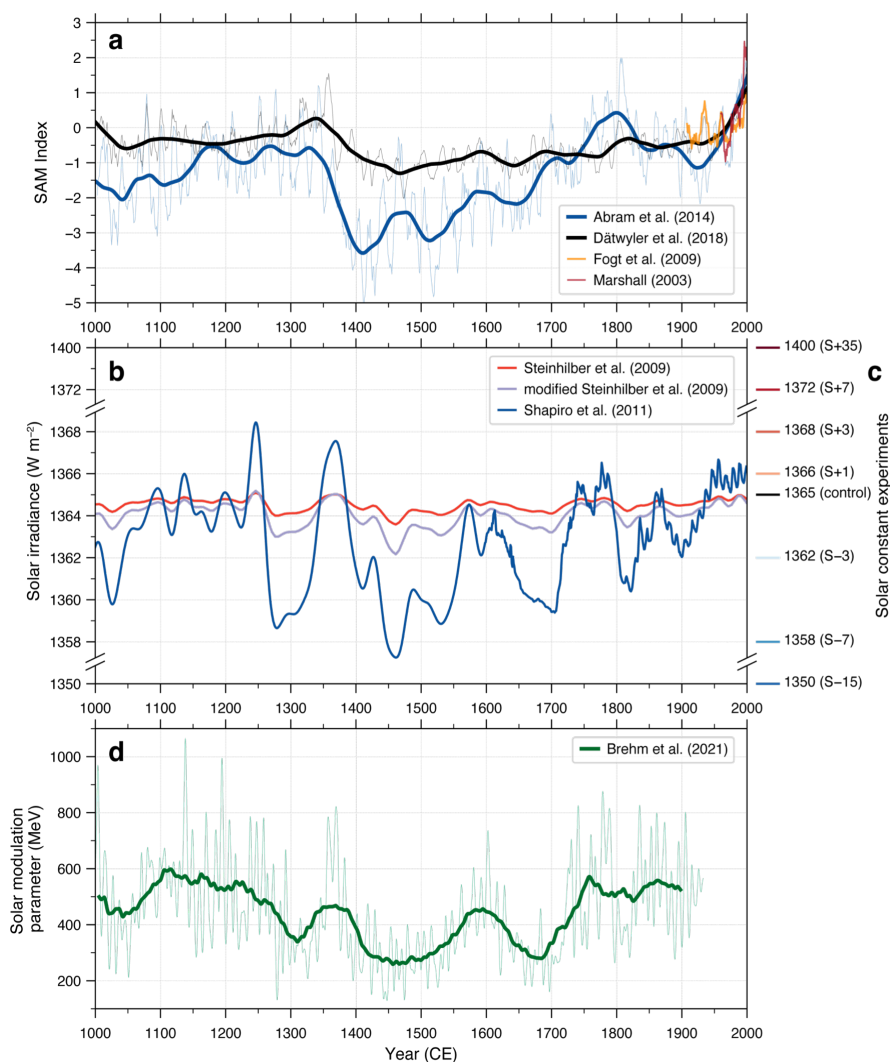




- 636 Visbeck, M.: A station-based southern annular mode index from 1884 to 2005, *Journal of Climate*, 22, 940-950,  
637 2009.
- 638 Wang, G. and Cai, W.: Climate-change impact on the 20th-century relationship between the Southern Annular  
639 Mode and global mean temperature, *Scientific reports*, 3, 1-6, 2013.
- 640 Wang, Y.-M., Lean, J., and Sheeley Jr, N.: Modeling the Sun's magnetic field and irradiance since 1713, *The*  
641 *Astrophysical Journal*, 625, 522, 2005.
- 642 Yang, D., Arblaster, J. M., Meehl, G. A., England, M. H., Lim, E.-P., Bates, S., and Rosenbloom, N.: Role of  
643 tropical variability in driving decadal shifts in the Southern Hemisphere summertime eddy-driven jet,  
644 *Journal of Climate*, 33, 5445-5463, 2020.
- 645 Zheng, F., Li, J., Clark, R. T., and Nnamchi, H. C.: Simulation and projection of the Southern Hemisphere annular  
646 mode in CMIP5 models, *Journal of Climate*, 26, 9860-9879, 2013.
- 647



648 **Figures**

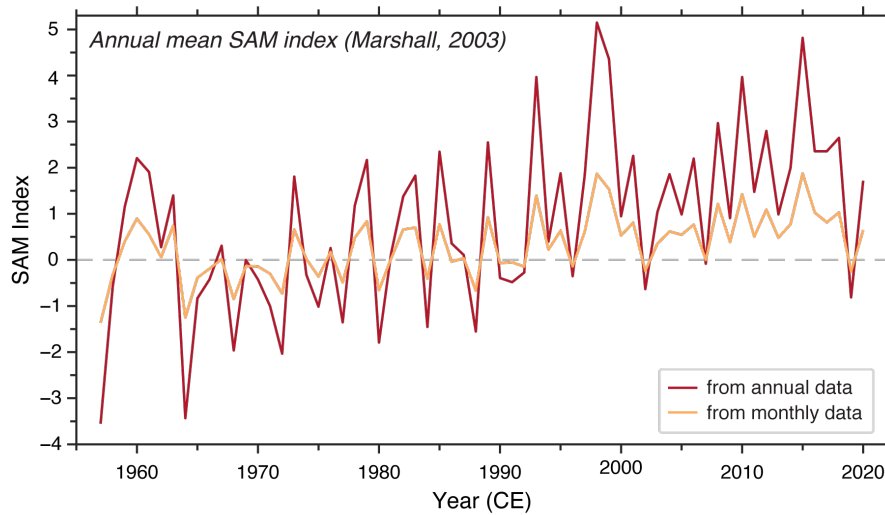


649

650 **Fig. 1. Reconstructed SAM and solar variability over the last millennium.** (a) Observation-based mean annual SAM  
651 indices (normalised units) of Marshall (2003) (red) and Fogt et al. (2009) (orange), and the reconstructed SAM index of  
652 Abram et al. (2014) (A14, blue) and Dätwyler et al. (2018) (D18, black; see Section 2.1 for an explanation of the  
653 difference in magnitude between the SAM reconstructions). The reconstructions are plotted as a 7-yr moving average  
654 for the annual SAM index (thin lines) with a 70-yr loess filter (thick lines), while 7-yr moving averages are shown for the  
655 observational data. (b) Total solar irradiance reconstructions for the last millennium, including Steinhilber et al. (2009)  
656 (red), Shapiro et al. (2011) (blue), and a modified version of Steinhilber et al. (2009) (purple) where the amplitude of the  
657 variations relative to the long-term mean has been increased by a factor of two. (c) Solar irradiance values for our solar  
658 constant experiments, with the experiment name provided in parentheses. (d) Solar modulation parameter  
659 reconstruction for the last millennium, based on radiocarbon from annually resolved and dated tree rings (Brehm et al.,  
660 2021), shown as monthly resolution (thin lines) and as a 70-yr moving average (thick lines).

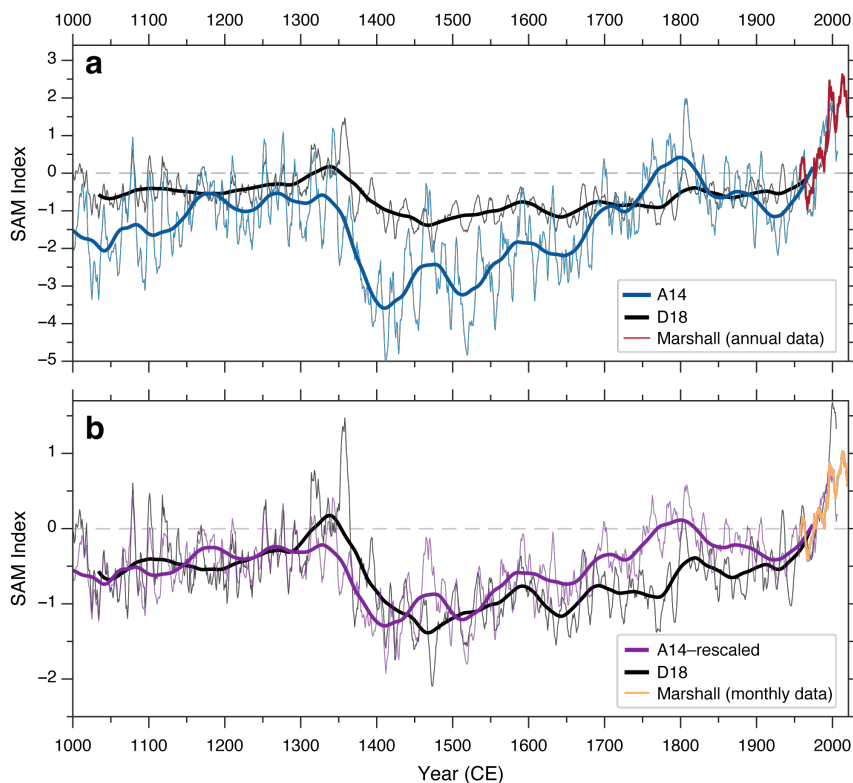


661



662

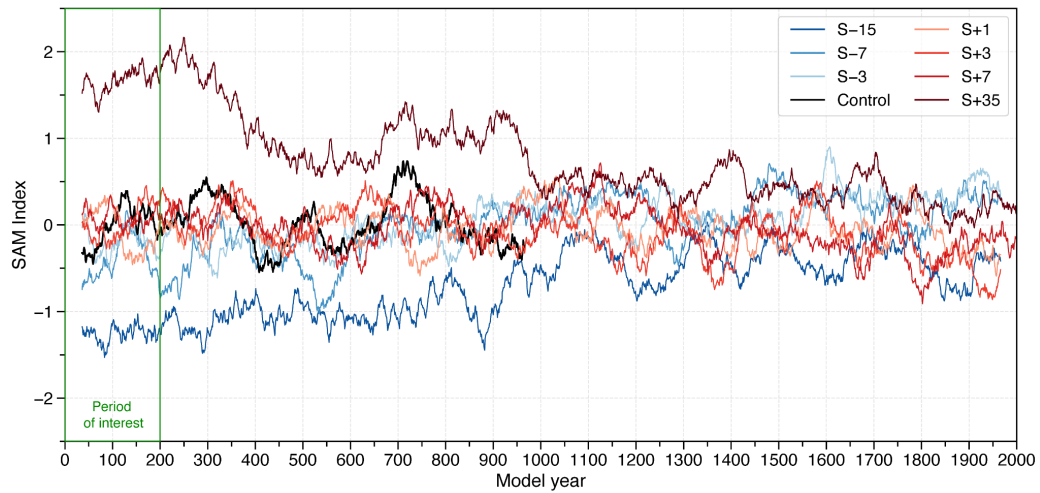
663 **Fig. 2.** Difference in the observed annual SAM index when calculated using monthly MSLP anomalies (i.e., using  
664 normalised monthly MSLP anomalies at 40°S and 65°S, and then averaging this monthly SAM index into an annual  
665 timeseries; orange line) and annual MSLP (i.e., normalised MSLP anomalies at 40°S and 65°S; red line). Data from  
666 Marshall (2003), and the updated index is publicly available (<http://www.nerc-bas.ac.uk/icd/gima/sam.html>).



667

668 **Fig. 3. The effect of calibration target on scaling of last millennium SAM reconstructions.**

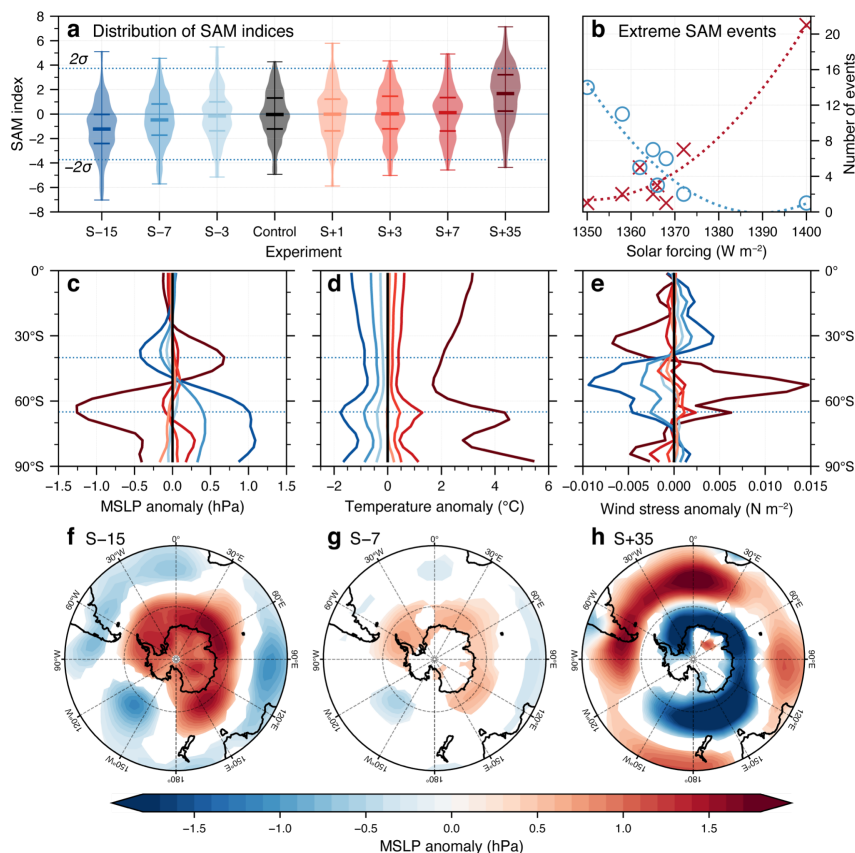
669 (a) observational-based annual SAM index (Marshall, 2003) calculated using annual MSLP anomalies (red line; shown as  
670 7-yr moving average), which forms the calibration target for the A14 SAM reconstruction (blue line; shown as 7-yr  
671 moving average and 70-yr loess filter by thin and thick lines, respectively). (b) observational-based annual SAM index  
672 (Marshall, 2003) calculated using monthly MSLP anomalies (orange line; shown as 7-yr moving average) and the result  
673 this alternate calibration target has on the scaling of A14 SAM reconstruction (purple line; shown as 7-yr moving  
674 average and 70-yr loess filter by thin and thick lines, respectively). For comparison, the D18 SAM reconstruction is  
675 shown in black (7-yr moving average and 70-yr loess filter by thin and thick lines, respectively) on both (a) and (b), and  
676 is based on a monthly-derived annual SAM index as the calibration target.



677

678 **Fig. 4. 70-yr moving average for the annual SAM index for each solar constant simulation. Period of interest in this**

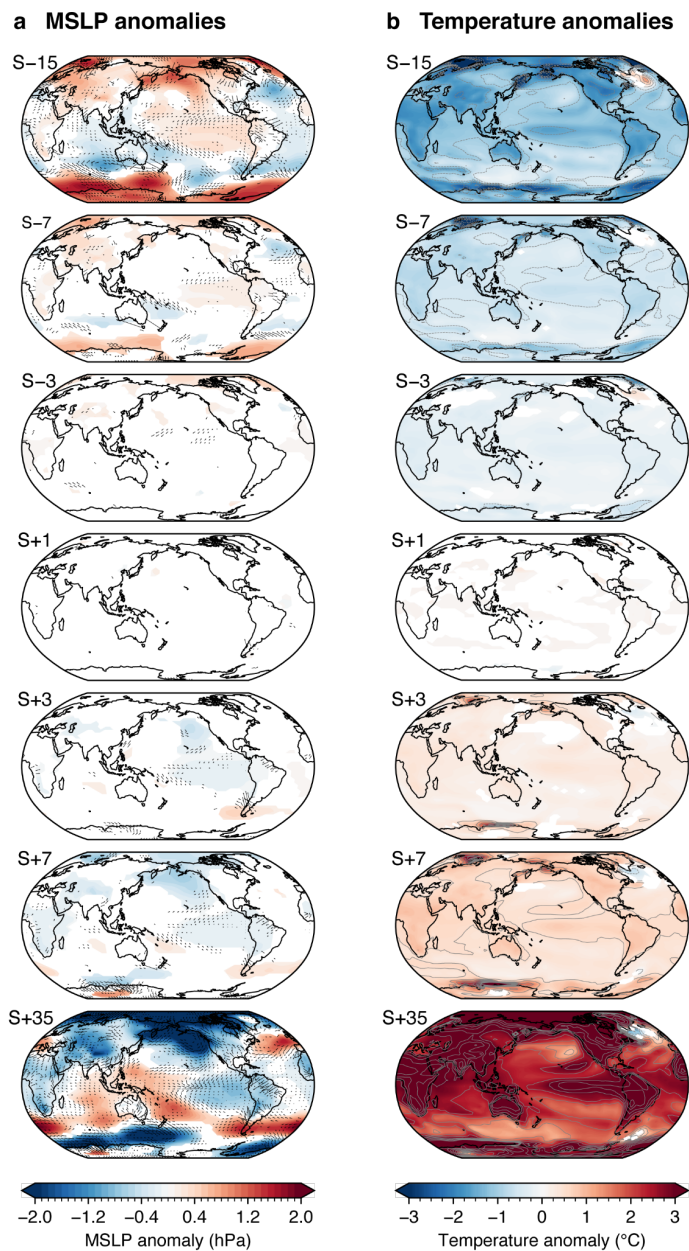
679 study (first 200 years) is indicated with a green box.



680

681 **Fig. 5: SAM index and events for the first 200 years of fixed solar forced model runs.**

682 (a) Violin plots of the distribution of mean annual SAM index calculated for each solar constant run. Coloured horizontal  
 683 lines refer to the 25th percentile, mean, and 75th percentile. (b) Number of extreme SAM events (outside  $\pm 2\sigma$  of the  
 684 control run) in 200 years, with a second order line of best fit for positive and negative events. Blue circles refer to  
 685 extreme negative SAM events, and red crosses refer to extreme positive SAM events. (c–e) Zonal mean anomalies for  
 686 the first 200 years of the experiments for: (c) mean sea level pressure, (d) surface air temperature, and (e) surface zonal  
 687 wind stress (positive values indicate westerly anomalies); where the anomaly is relative to the control run. Colours for  
 688 each experiment correspond to those used in panel (a). Dashed lines at  $40^\circ\text{S}$  and  $65^\circ\text{S}$  are the latitudes used to  
 689 calculate the SAM index. (f–h): MSLP anomalies relative to the control for the first 200 years in the (f) S–15, (g) S–7,  
 690 and (h) S+35 experiments. Regions shown are significantly different to the control run (based on Welch’s t-test,  
 691  $P < 0.05$ ); areas where  $P \geq 0.05$  have been masked out.



692

693

694

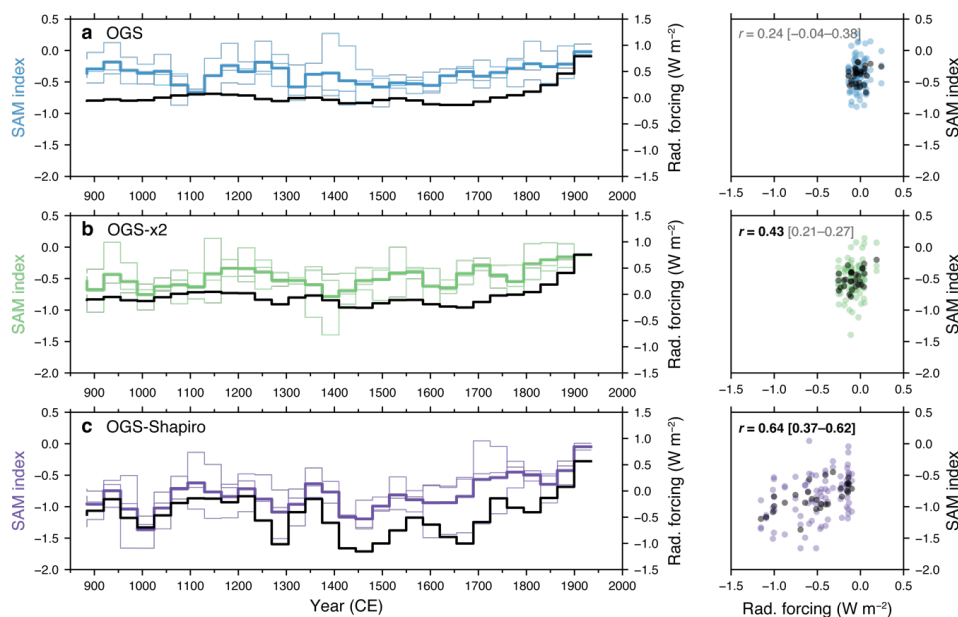
695

696

697

**Fig. 6. Surface anomalies (relative to the control run) for the first 200 years of the different solar constant experiments.** (a) MSLP anomaly (shaded) and surface wind anomalies (vectors). (b) Surface temperature anomaly (shaded), with temperature contours additionally shown at 0.5 °C increments (to assist in interpreting S+35). Regions that are significantly different (based on a Welch's *t*-test,  $P < 0.05$ ) are shown, while areas where  $P \geq 0.05$  have been masked out.





698

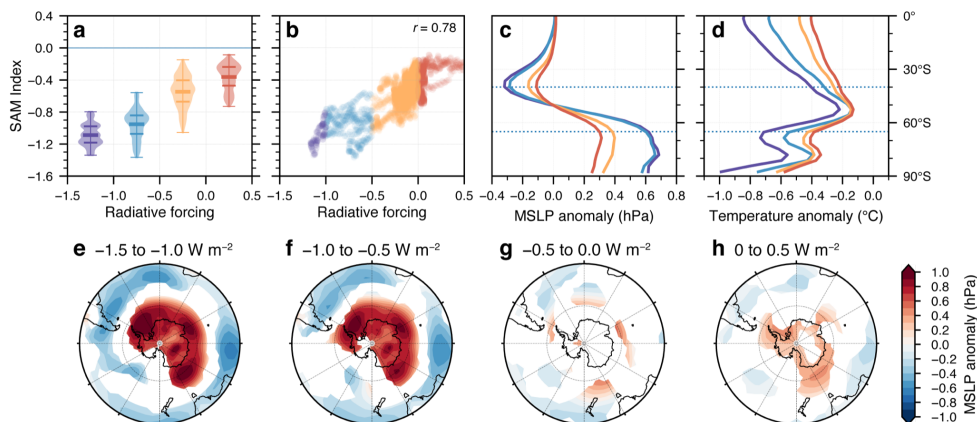
699 **Fig. 7: SAM index response to different amplitudes of transient solar forcing during the last millennium.** Time  
700 series (left-side panels) of the SAM index (coloured lines; ensemble mean: thick line; ensemble members: thin lines) and  
701 radiative forcing anomalies (black) in the transient experiments with (a) low, (b) intermediate and (c) large amplitude  
702 solar forcing. Time series shown for the SAM index are calculated relative to 1900–1999 climatology, and long-term  
703 changes are represented as 70-yr moving averages stepped by 35 years. Scatter plots (right-side panels) show the  
704 850–1900 CE correlation between 70-yr moving averages stepped by 35 years of the SAM index and radiative forcing  
705 anomalies in the ensemble mean (black, first  $r$ -value), and ensemble members (coloured,  $r$ -values in square brackets  
706 give range across ensemble members);  $r$ -values in bold text are where  $P < 0.05$ , while  $r$ -values in grey text are where  
707 there is no significant relationship. Correlations are limited to 850–1900 CE to avoid the influence of recent  
708 anthropogenic greenhouse gas influences on the radiative forcing–SAM relationship.

709



710

711

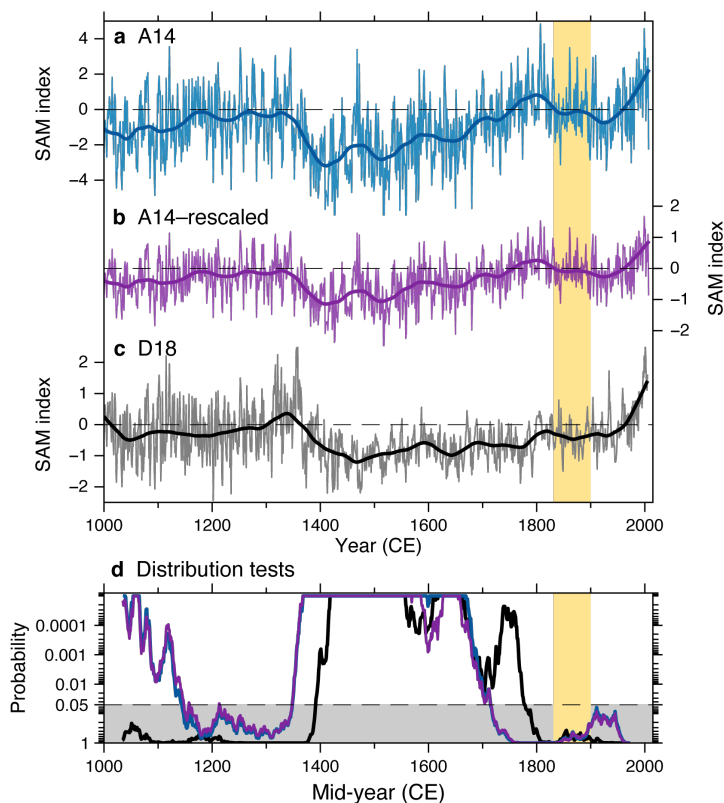


712

713

714 **Fig. 8: SAM index response to different levels of radiative forcing compiled across solar transient experiments.**

715 (a) Violin plots of the 70-yr rolling mean SAM index between 850–1900 CE; lines refer to the 25th percentile, mean, and  
716 75th percentile. (b) Scatter plot of 70-yr rolling mean for radiative forcing anomaly and the SAM index;  $r = 0.78$   
717 ( $P < 0.05$ ). (c–d) Zonal mean anomalies for: (c) mean sea level pressure (MSLP), and (d) temperature, where the anomaly  
718 is relative to the climatological (1900–1999) mean. Coloured lines refer to the radiative forcing bins for  $-1.5$  to  
719  $-1.0 \text{ W m}^{-2}$  (purple),  $-1.0$  to  $-0.5 \text{ W m}^{-2}$  (blue);  $-0.5$  to  $0.0 \text{ W m}^{-2}$  (orange);  $0.0$  to  $0.5 \text{ W m}^{-2}$  (red). (e–h) MSLP anomalies  
720 (relative to the climatological mean based on radiative forcing bins). Regions shown are significantly different to the  
721 OGS ensemble mean (based on Welch's t-test,  $P < 0.05$ ); areas where  $P \geq 0.05$  have been masked out. Dashed lines at  
722  $40^\circ\text{S}$  and  $65^\circ\text{S}$  are the latitudes used to calculate the SAM index.

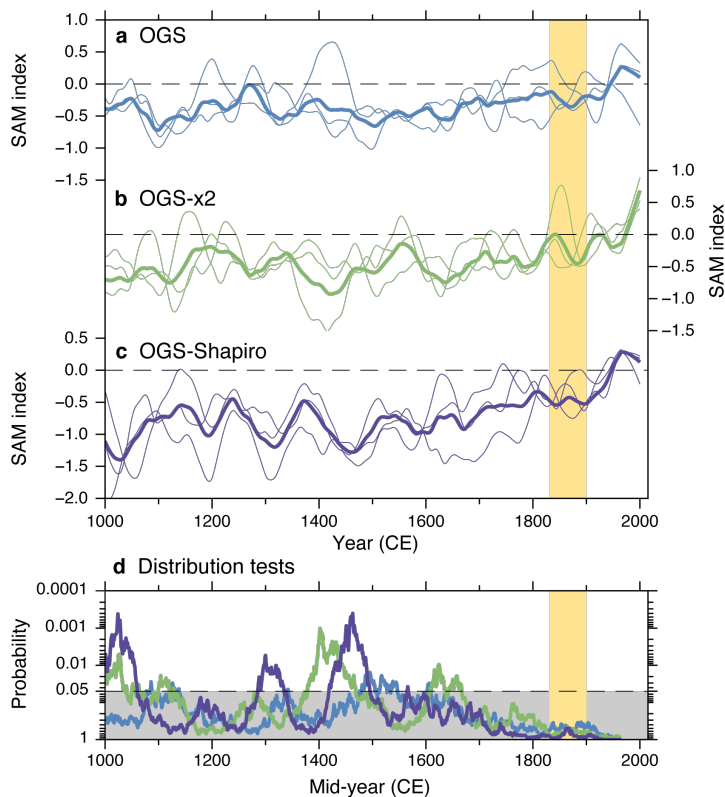


723

724 **Fig. 9. Last millennium SAM reconstructions (a–c) and the significance of negative shifts in 70-year distributions**  
725 **through time relative to a 70-yr preindustrial reference period (1831–1900) (d).** Annual mean SAM reconstructions  
726 (thin curves) and 70-y loess filters (thick curves) for (a) the A14 SAM reconstruction (blue); (b) the A14-rescaled SAM  
727 reconstruction (purple; See Fig. 3); and (c) the D18 SAM reconstruction. SAM reconstructions shown relative to 1900–  
728 1999 climatology (dashed horizontal lines) (d) Distribution tests using a Wilcoxon rank-sum test of moving 70-yr  
729 windows of each SAM reconstruction shown in parts (a–c), relative to its 70-year preindustrial reference period (1831–  
730 1900 CE; yellow vertical shading). Timeseries show the probability for the distribution of sliding test windows being  
731 more negative than the distribution in the reference interval;  $P < 0.05$  are shown with a white background, while  $P \geq$   
732  $0.05$  are shown with a grey background. All three reconstructions show a significant ( $P < 0.05$ ) negative shift in the SAM  
733 index compared with the 1831–1900 reference interval during the period from approximately 1390 to 1715 CE. Both  
734 versions of the A14 SAM reconstruction also have a significant negative SAM shift prior to around 1140 CE.

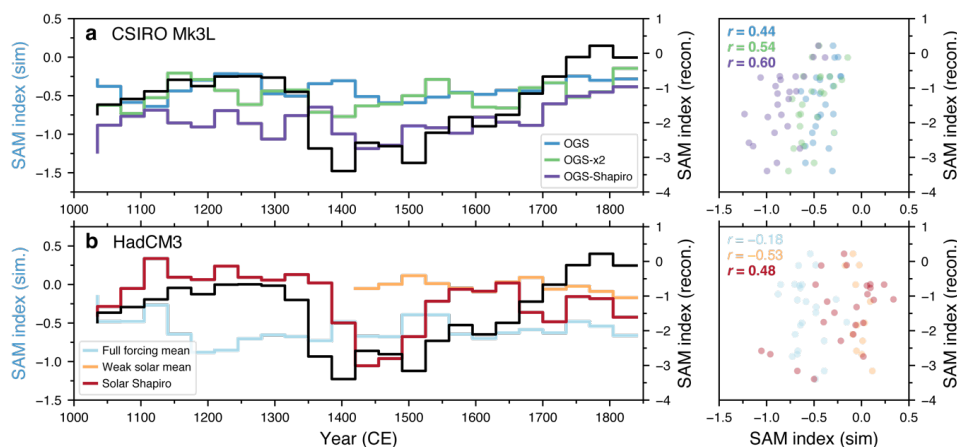


735



736

737 **Fig. 10. SAM index in the CSIRO Mk3L transient last millennium simulations (a–c) and the significance of**  
738 **negative shifts in 70-year windows of annual SAM distributions through time relative to a 70-yr preindustrial**  
739 **reference period (1831–1900) (d).** 70-yr loess filter of the SAM index of (a) the OGS simulations; (b) OGS-x2  
740 simulations; and (c) OGS-Shapiro simulations (as in Fig. 7). The ensemble mean is shown as a thick line, and individual  
741 ensemble members are shown in thin lines. SAM indices are shown relative to their 1900–1999 climatology (dashed  
742 horizontal lines). (d) Distribution tests on ensemble means using a Wilcoxon rank-sum test of sliding 70-yr windows  
743 relative to the preindustrial reference period (1831–1900 CE; vertical yellow shading), where colours match the SAM  
744 simulations shown in parts a–c. Timeseries show the probability for the distribution of sliding test windows being more  
745 negative than the distribution in the reference interval.  $P < 0.05$  are shown with a white background, while  $P \geq 0.05$  are  
746 shown with a grey background.



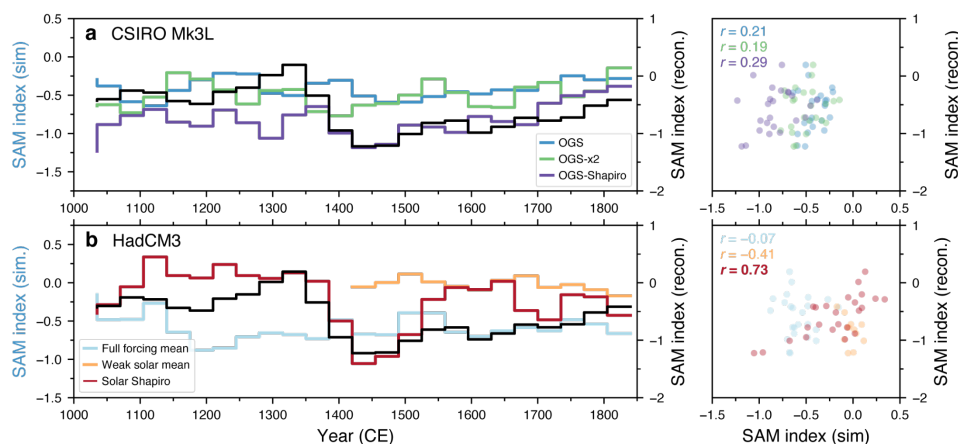
747

748 **Fig. 11: Comparison of simulated SAM index and the A14 SAM reconstruction between 1000 and 1900 CE.** Time  
749 series (left-side plots) of the SAM index (70-yr moving averages stepped by 35 years, calculated relative to 1900–1999  
750 historical mean) from ensemble means of transient simulations and SAM reconstructions (black line; A14) (a) for  
751 transient experiments from CSIRO Mk3L using low (blue, OGS), intermediate (green, OGSx2), and high (purple, OGS-  
752 Shapiro) amplitude solar forcing. (b) for simulations from HadCM3 (Schurer et al., 2014), including the full forcing (blue),  
753 weak solar (orange) and strong solar ('Solar Shapiro' runs using Shapiro et al., 2011; red) simulations. Note that there is  
754 only a single member for the strong solar scenario, and that the solar forcing simulations from HadCM3 do not include  
755 greenhouse gases whereas the full forcing simulation does. This results in the last millennium SAM index from the full-  
756 forcing simulation having a lower mean than the solar forcing-only experiments when calculated relative to the 1900–  
757 1999 historical mean. Scatter plots (right-side plots) show the correlation between the simulated ensemble mean and  
758 reconstructed SAM indices, as 70-yr moving averages stepped by 35 years, and  $r$ -values between the simulated and  
759 reconstructed SAM index are shown in bold text where  $P < 0.05$ .



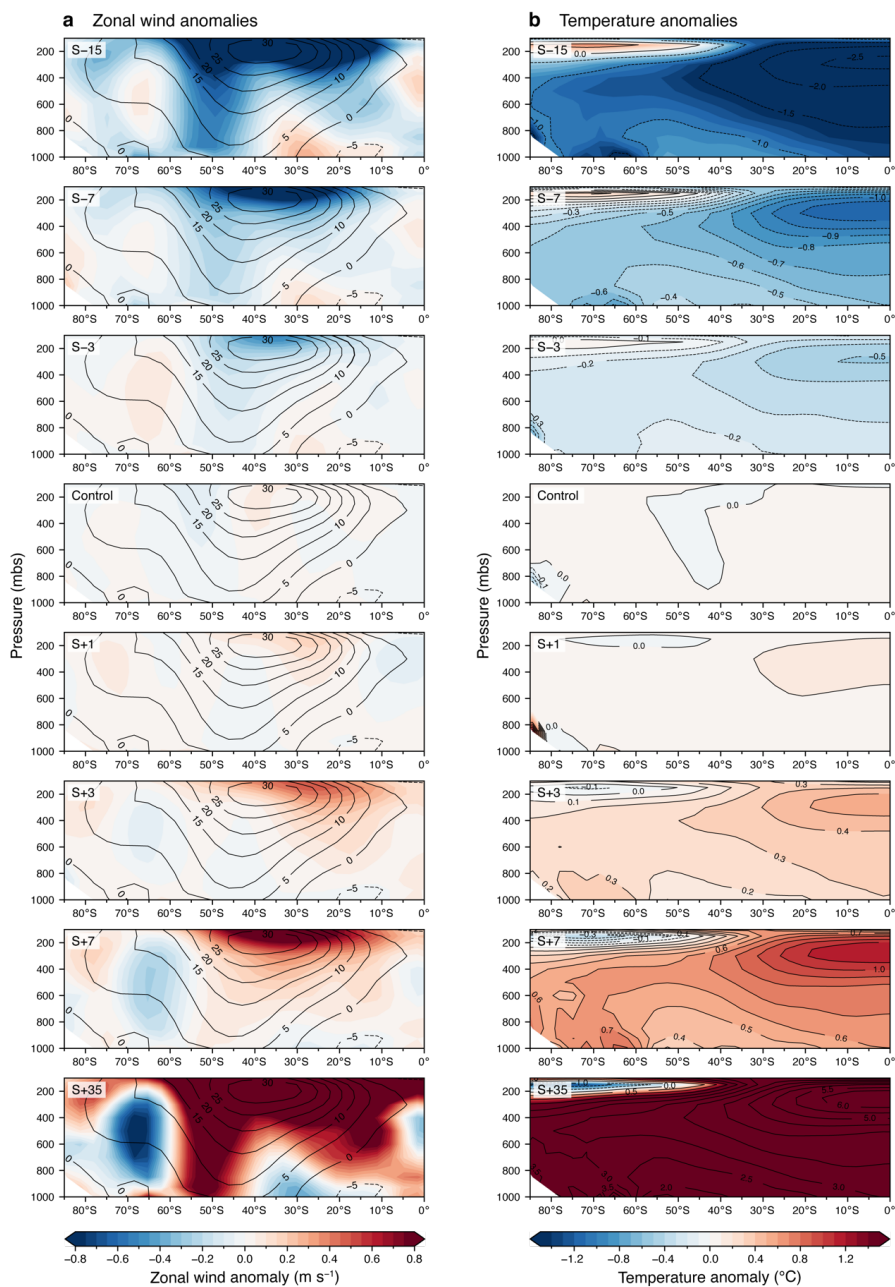
760

761



762

763 **Fig. 12: Comparison of simulated SAM index and the D18 SAM reconstruction between 1000 and 1900 CE.** Time  
764 series of the SAM index (70-yr moving averages stepped by 35 years; ensemble mean: thick line; ensemble members:  
765 thin lines) from transient simulations and SAM reconstruction (70-yr moving averages stepped by 35 years) from D18  
766 (black line) for (a) solar transient experiments from CSIRO Mk3L, and (b) simulations from HadCM3 (Schurer et al.,  
767 2014), including the full forcing (blue), weak solar (orange) and strong solar (i.e., Shapiro et al., 2011; red) simulations.  
768 Note that the solar forcing simulations from HadCM3 do not include GHGs. Scatter plots show the correlation between  
769 70-yr moving averages of the simulated SAM index and 70-yr moving average of the reconstructed SAM index for the  
770 ensemble mean, and  $r$  values between the simulated and reconstructed SAM index where  $P < 0.05$  are shown in bold  
771 text.



772

773 **Fig. 13: Atmospheric profiles for the Southern Hemisphere mean anomalies for the first 200 years of each solar**

774 **constant experiment.** Anomalies are calculated relative to the long-term control. (a) Zonal wind anomalies (shaded),

775 and contours of the control zonal wind (lines). (b) Temperature anomalies (shaded); contour lines of the temperature

776 anomaly are additionally shown in  $0.5^{\circ}\text{C}$  increments, to assist in interpreting S-15 and S+35.